
Article:
Sayegh, AS orcid.org/0000-0002-9810-2915, Connors, RD orcid.org/0000-0002-1696-0175 and Tate, JE orcid.org/0000-0003-1646-6852 (2018) Uncertainty propagation from the cell transmission traffic flow model to emission predictions: a data-driven approach. Transportation Science, 52 (6). pp. 1327-1346. ISSN 0041-1655

https://doi.org/10.1287/trsc.2017.0787

Uncertainty propagation from the cell transmission traffic flow model to emission predictions: a data-driven approach

Arwa S. SAYEGH[1], Richard D. CONNORS[1], and James E. TATE[1]
[1]*Institute for Transport Studies, University of Leeds, Leeds, UK LS2 9JT*

ABSTRACT

Road traffic exhaust emission predictions are used to inform transport policy and investment decisions aimed at reducing emissions and achieving sustainable mobility. Emission predictions are also used as inputs when modelling air quality and human exposure to traffic-related air pollutants. To be effective, such policies and/or integration must be based on robust models that not only provide point-based predictions, but also inform these with an interval of confidence that properly accounts for the propagation of uncertainties through the complex chain of models involved. This paper develops a data-driven methodological framework which enables calculating the uncertainty in average speed-based emission predictions induced by uncertainty in its traffic data inputs which are most often predictions (or outputs) of traffic flow models. An ensemble-based optimisation approach is used to estimate both calibration and validation errors arising from uncertainty in the structure and parameterisation of the Cell Transmission Model (CTM); a discretised first-order macroscopic traffic flow model that is often integrated with average speed-based emission models. A Monte Carlo sampling approach is proposed to propagate the uncertainty in traffic flow inputs to emission predictions. To ensure transferability of findings, this methodology has been tested using multiple real data sets on three motorway road networks, one of which operates under Variable Speed Limits (VSL).

Keywords: modelling chain, ensemble-based optimisation, traffic-related air pollutants, calibration and validation, error estimation, Monte Carlo.

1. Introduction

Human exposure to harmful road traffic-related air pollutants can, in principle, be assessed using direct measurements of roadside air quality. However, in many current scenarios and particularly for

forecasting and policy development, modelling is required. The key inputs to physical ambient air quality models are source emission measurements, estimates, or predictions. While many sources of emissions contribute to air quality, this paper focusses only on those arising from road traffic. Road traffic exhaust emissions can either be measured directly or estimated using road traffic activity data. However, the limited spatial and temporal resolution of measurements of both exhaust emissions and traffic activity often leads to the use of traffic flow models to provide the dynamic traffic density/flow/speed along the link i.e. the inputs required by emission models. This results in a complex four-step modelling chain, traffic flow – exhaust emission – ambient air quality – human exposure, founded upon traffic flow models and their integration with traffic emission models.

It is worth noting that, particularly in the case of future forecasts, the traffic (in)flow level on a particular road link may come not from direct measurement, but from a traffic assignment model that distributes travel demand on a (complex) road network accounting for the route choice of individual drivers. This would give rise to additional uncertainties within an even more complex five-step modelling chain, but is outside the scope of this paper.

Various approaches have been developed to integrate traffic flow and emission models, depending on the level of detail desired in emission predictions; Wismans et al. (2011) and Shorshani et al. (2015) provide a comprehensive review. Perhaps the two most straightforward approaches are: whole-link traffic flow models (also referred to as static macroscopic traffic flow models) with average speed-based emission models (e.g. Namdeo et al. 2002; or Nejadkoorki et al. 2008); and microscopic traffic flow models with instantaneous or power-based emission models (e.g. Rakha and Ahn 2004; or Int Panis et al. 2006). However, macroscopic traffic flow models, which represent traffic as a continuum and consider only aggregate traffic behaviour, have recently been integrated with different types of emission models in an attempt to improve on the low-fidelity of whole-link traffic flow models while avoiding the high costs associated with microscopic traffic flow models in terms of their computation, data requirements, and calibration.

Continuum-based macroscopic traffic flow models can take different forms and are typically distinguished based on the number of equations involved in describing the dynamics of traffic

variables (mainly traffic density, traffic flow, and traffic speed). For instance, the Lighthill-Whitham-Richards (LWR)-type models (Lighthill and Whitham 1955a, 1955b; Richards 1956) are governed by a non-linear partial differential equation that describes the dynamics of traffic density and considers a steady-state relationship between average traffic density and traffic speed referred to as the fundamental diagram. LWR-type models are referred to as first-order macroscopic traffic flow models. Payne-type models (Payne 1971) and Helbing-type models (Helbing 1996), however, are governed by two and three partial differential equations, respectively, and allow for variations around traffic speeds implied by the fundamental diagram. Despite the limitation of LWR-type models – such as assuming that the average speed adapts instantaneously to traffic density without considering any delay (Hoogendoorn and Bovy 2001) – they are commonly used in a number of fields such as traffic control optimisation on motorways (e.g. Gomes et al. 2008; Hadiuzzaman and Qiu 2013; and Li et al. 2015), traffic signal optimisation on urban roads (e.g. Feldman and Maher 2002), and evacuation planning (e.g. Kimms and Maassen 2011). Most recently, they have also been used for predicting exhaust emissions as a result of their simplicity and rigorousness in terms of parameterisation and the physical meaning of the parameters involved.

Cell Transmission Model (CTM) (Daganzo 1994, 1995), in particular, has been used in a number of studies to predict space-time varying average speed-based emissions (e.g. Lin and Ge 2006; Zhu et al. 2013; Samaranayake et al. 2014) or driving-mode based emissions (e.g. Zhang et al. 2013). Most of these studies have used predicted emissions based on CTM in order to predict air quality levels (Lin and Ge 2006; Samaranayake et al. 2014) or even exposure levels (Zhang et al. 2013). Zhang et al. (2013) formulated a bi-objective optimisation framework to determine signal timings which minimises traffic delay and the risk associated with human exposure to traffic emissions. Similarly, Liu et al. (2014) proposed a multi-class form of CTM and developed a model-based control framework which optimises motorway traffic control systems by minimising both total travel times and total instantaneous-based emissions predicted indirectly using their traffic flow model. That said, calibration (or optimisation) and validation studies of CTM are rather limited; see Muñoz et al. (2004), Dervisoglu et al. 2009, Spiliopoulou et al. (2014), Gkiotsalitis and Chow (2014), and Zhong et

al. (2015). Alternatively, Zhou et al. (2015) have integrated Newell's macroscopic traffic flow model (Newell 1993) with a simple linear car-following model proposed also by Newell (2002) to generate vehicle trajectories and consequently predict instantaneous-based emissions. Both CTM and Newell's macroscopic traffic flow model are simplified variations of the LWR model, with traffic state variables discretised into short road segments (often referred to as cells) and time steps.

While the use of LWR-type models to predict emissions is well established, uncertainty around the emission predictions is yet to be understood. Despite their focus on exposure assessment models, Cullen and Frey (1999) emphasised that uncertainty arises due to limited availability of empirical information and/or imperfections in developed complex physical modelling systems and thus it is essential to not only report point-based predictions based on such models but also probabilistic predictions based on an understanding of the sources of uncertainty and their propagation to the final modelling outputs. Such concerns directly motivate this paper. For the case of LWR-based emission predictions, complex sources of uncertainty arise from the input, parameterisation, and involved model structures; studying their propagation to the final emission predictions to allow reporting not only a point-based emission prediction but also the uncertainty around each point is thus essential.

Few studies on the uncertainty in LWR-type models and emission models have been made, separately. While many have focussed on developing variations of existing LWR-type models which incorporate uncertainties in input and parameterisation (e.g. Sumalee et al. 2011; Ngoduy 2011), Li et al. (2012) took another approach and focussed on whether predictions from LWR can be trusted given uncertainties in the free-flow traffic speed parameter of the fundamental diagram. They assumed that this particular parameter cannot be perfectly specified, given the limitations of the LWR model. Alternatively, Kühlwein and Friedrich (2000) have investigated uncertainties in traffic situation emission predictions based on uncertainties in the model inputs such as emission factors, traffic volume, and vehicle proportions. Kini and Frey (1997) (also summarised in Cullen and Frey (1999) as a case study) studied key sources of uncertainty in the USEPA average speed-based emission model (MOBILE5) and developed a probabilistic version of selected components of the

model in order to not only report point-based predictions but also uncertainty in emission predictions. The present paper integrates the well-developed and commonly used CTM and average speed-based emission models in order to not only study uncertainties in key components of a single step of the overall modelling chain, but also to study uncertainty propagation from CTM to average speed-based emission predictions. Specifically, this study focusses on both capturing uncertainty in the model structure of CTM and parameterisation, and propagating it to average speed-based emission predictions.

This paper develops a data-driven methodological framework to uncertainty propagation in the modelling chain: using an ensemble-based approach to optimisation (for parameter estimation) and error estimation of calibrated and validated models allows capturing uncertainty in CTM model structure and parameters. A Monte Carlo sampling approach allows for the quantification of this uncertainty in CTM model outputs, and thus its propagation to emission predictions. This paper uses three real motorway road networks and multiple real data sets to test the applicability of the developed methodology and transferability of results. One of the road networks is operated on Variable Speed Limits (VSL) which requires the use of a variation of CTM model formulation. While VSL-modified macroscopic traffic flow models have been developed, calibration and validation studies of them are still limited. The paper thus allows assessing its performance using real-data while also comparing the application of the developed methodology on both the basic CTM model formulation and VSL-modified CTM model formulation.

2. Data-driven methodology

2.1. CTM-based emission predictions

The original CTM formulation (Daganzo 1994, 1995) modelled the dynamics of occupancy (i.e. number of vehicles) at each cell of a road network; a cell being a short segment of a road network link. This formulation required equal cell lengths. By using cell density instead of occupancy, Muñoz et al. (2004) formulated a CTM allowing uneven cell lengths. In general, given input data and model

parameters, the outputs of CTM are predicted traffic density (ρ), traffic flow (q), and traffic speed (u), each a 2-D matrix capturing the space-time dynamics of these variables at every predefined discretised cell and time step. This can be summarised by **Eq. 1** where Z comprises the three output matrices of traffic variables; f is the CTM function (or model structure); $\tilde{I}$ is the model input data; and $\tilde{Z}$ is the real traffic data necessary for calibration of the CTM parameter vector β. In this paper, any *measured* variable X is annotated by $\tilde{X}$. While traffic assignment models can be used to distribute and assign traffic demand to different network paths, hence providing link inflows that feed into CTM as model input data (e.g. as proposed in Lo and Szeto 2002), this study rather focusses on using real measurements as input data.

$$Z = (\rho, q, u) = f[\tilde{I}, \beta(\tilde{Z})] \quad \textbf{(1)}$$

The road network is partitioned into short cells of length l_i $\{i = 1,2, \dots, N\}$ where *i-1 = 0* represents mainline origin and *i+1 = N+1* represents mainline destination. CTM allows for the calculation of traffic density [veh km^{-1} lane^{-1}] at each cell i and time step t $\{t = 1,2, \dots, T\}$ where T is the total number of time steps, using two recursive equations: the conservation law and the fundamental diagram (FD). A triangular FD was initially proposed by Daganzo (1994), and was then relaxed to a trapezoidal FD in Daganzo (1995). The parameter vector of CTM trapezium is $\beta = (u_f, Q_{max}, w, \rho_{max})$ comprising the free-flow traffic speed [km h^{-1}], maximum traffic flow [veh h^{-1} lane^{-1}], backward-wave speed [km h^{-1}], and maximum traffic density [veh km^{-1} lane^{-1}], respectively, as shown in **Fig. 1a**. These FD parameters could be cell-specific, to reflect real differences between cells, however this can give rise to 'fake' results from the calibration of parameters based on limited data (Spiliopoulou et al. 2014). In this paper attention is restricted to scenarios where cells share the same (static) infrastructural characteristics, see **section 3**, and hence the FD parameters are assumed uniform across all cells.

CTM can be described as a combination of a link model and node model: a node is located wherever there is a change in geometry of a road network, i.e. at on-ramps requiring merge nodes and off-ramps requiring diverge nodes; and a link connects such nodes. A description of CTM for cells

on links without any merge or diverge nodes is provided by the following equations:

$$\rho_i(t+1) = \rho_i(t) + \frac{T_s}{l_i \lambda_i}\left[q_{i-1/2}(t) - q_{i+1/2}(t)\right] \quad (\mathbf{2})$$

$$q_{i+1/2}(t) = min\{S_i(t), R_{i+1}(t)\} \quad (\mathbf{3})$$

$$S_i(t) = min\{u_f \rho_i(t), Q_{max}\}\lambda_i;\ S_0(t) = d_0(t) \quad (\mathbf{4})$$

$$R_{i+1}(t) = min\{w[\rho_{max} - \rho_{i+1}(t)], Q_{max}\}\,\lambda_{i+1} \quad (\mathbf{5})$$

such that $w \leq u_f$; $Q_{max} \leq \frac{\rho_{max}}{\frac{1}{u_f}+\frac{1}{w}}$; and $u_f \leq \frac{min(l_i)}{T_s}$

Given initial traffic density for each cell $\rho_i(0)$, traffic demand from mainline origin $d_0(t)$, and traffic density at mainline destination $\rho_{N+1}(t)$, **Eq. 2** shows that traffic density $\rho_i(t)$ in any cell *i* with number of lanes λ_i can be updated according to the conservation law of vehicles: in time interval *[t,t+1]* of length T_s [h], $q_{i-1/2}(t)$ is the traffic inflow into cell *i* from cell *i-1* (or equivalently, the traffic flow at the cell interface *i-1/2*) and $q_{i+1/2}(t)$ is the traffic outflow from cell *i* into cell *i+1* in veh h^{-1} (or equivalently, the traffic flow at the cell interface *i+1/2*). Traffic inflows or outflows are calculated based on the FD using **Eq. 3**: the traffic outflow is the maximum sending capacity of the upstream cell *i* under free-flow conditions (**Eq. 4**) limited by the receiving capacity of the downstream cell *i+1* under congested conditions (**Eq. 5**). The three conditions represent the two properties of the trapezoidal FD plus the Courant–Friedrichs–Lewy condition (Daganzo 1995) that the minimum cell length needs to be longer than the free-flow distance to avoid instabilities in the model outputs.

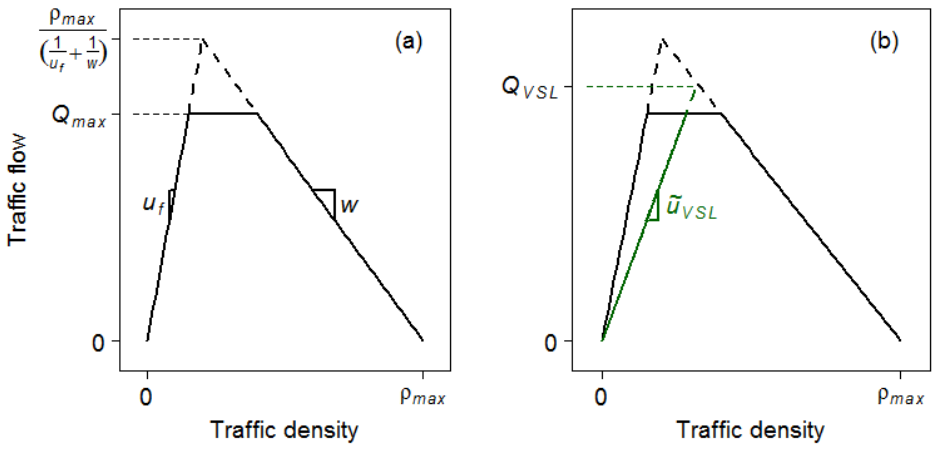

Fig. 1: traffic flow as a function of traffic density considered as the (a) CTM-basic fundamental diagram and (b) CTM-vsl fundamental diagram.

The above formulation describes the dynamics for cells without any on-ramps and off-ramps. On-ramps (or merge nodes) can be located at the upstream interface of a cell and off-ramps (or diverge nodes) can be located at the downstream interface of a cell. In the presence of an on-ramp at upstream cell interface *i-1/2* with traffic demand $d_{on,i-1/2}(t)$ in veh h^{-1}, there exist two scenarios: the first is when the downstream cell *i* can accommodate both the mainline cell *i-1* outflow and the on-ramp demand; and the second is when the mainline cell *i-1* outflow and on-ramp demand exceed the receiving capacity of the downstream cell *i*. In either cases, it is assumed that the on-ramp has unlimited capacity or at least that on-ramp traffic demand is lower than its capacity. The mainline outflow from cell *i-1* to cell *i*, $q_{i-1/2}(t)$, and the actual on-ramp outflow to cell *i*, $q_{on,i-1/2}(t)$, are calculated based on **Eq. 6** and **Eq. 7** accordingly,

$$q_{i-1/2}(t) = \begin{cases} S_{i-1}(t) & if\ S_{i-1}(t) \le R_i(t) - d_{on,i-1/2}(t) \\ max\left[0, R_i(t) - d_{on,i-1/2}(t)\right] & \text{otherwise} \end{cases} \quad (6)$$

$$q_{on,i-1/2}(t) = \begin{cases} d_{on,i-1/2}(t) & \text{if } S_{i-1}(t) \le R_i(t) - d_{on,i-1/2}(t) \\ R_i(t) - q_{i-1/2}(t) & \text{otherwise} \end{cases} \quad (7)$$

In the presence of an off-ramp at downstream cell interface *i+1/2*, it is assumed that the off-ramp has unlimited capacity and the traffic outflow of **Eq. 3** is modified to **Eq. 8** where $\theta_{i+1/2}(t)$ represents the split ratio of the off-ramp. The traffic outflow to the off-ramp can then be calculated

based on **Eq. 9**.

$$q_{i+1/2}(t) = min\{[1 - \theta_{i+1/2}(t)]\, S_i(t), R_{i+1}(t)\} \quad (8)$$

$$q_{off,i+1/2}(t) = \theta_{i+1/2}(t)\, \frac{q_{i+1/2}(t)}{1-\theta_{i+1/2}(t)} \quad (9)$$

In the presence of both an on-ramp and off-ramp on cell *i*, **Eq. 2** is updated to take into account on-ramp inflows and off-ramp outflows as shown in **Eq. 10** below.

$$\rho_i(t+1) = \rho_i(t) + \frac{T_s}{l_i \lambda_i}\left[q_{i-1/2}(t) + q_{on,i-1/2}(t) - q_{i+1/2}(t) - q_{off,i+1/2}(t)\right] \quad (10)$$

CTM traffic speed can be calculated either at the cell interfaces or within the cells. At cell interfaces the calculation involves traffic inflows/outflows and traffic density; the resulting traffic speed does not necessarily follow the FD. Within a cell, traffic speed is calculated using the FD. Space-mean traffic speed of cell *i* at time step *t* is thus calculated using **Eq. 11**.

$$u_i(t) = \frac{q_i(t)}{\rho_i(t)\lambda_i} = \frac{min\{S_i(t), R_i(t)\}}{\rho_i(t)\lambda_i} = \frac{min\{u_f \rho_i(t), Q_{max}, w[\rho_{max} - \rho_i(t)]\}}{\rho_i(t)} \quad (11)$$

In addition to the above, Liu et al. (2014) have proposed using a simple queue model at the mainline and on-ramp origins in order to ensure that the entire traffic demand is entering the network in the case when traffic outflows are restricted by the receiving capacity of the cell at which an origin is located. The queue model is given by **Eq. 12** and **Eq. 13** where $h_{on,i-1/2}(t)$ represents the queue length at time step *t* of the on-ramp located at upstream cell interface *i-1/2* and $\acute{d}_{on,i-1/2}(t)$ represents the updated traffic demand depending on the queue length. The updated traffic demand needs to also be used in **Eq. 6** and **Eq. 7** instead of $d_{on,i-1/2}(t)$. **Eq. 12** and **Eq. 13** are similarly applied for the mainline origin with traffic demand $d_0(t)$, traffic inflow $q_{1-1/2}(t)$, and queue length $h_{1-1/2}(t)$.

$$h_{on,i-1/2}(t+1) = h_{on,i-1/2}(t) + T_s\left[\acute{d}_{on,i-1/2}(t) - q_{on,i-1/2}(t)\right] \quad (12)$$

$$\acute{d}_{on,i-1/2}(t) = d_{on,i-1/2}(t) + \frac{h_{on,i-1/2}(t)}{T_s};\ h_{on,i-1/2}(0) = 0 \quad \textbf{(13)}$$

Few studies have extended the basic CTM to account for VSL operation. While Hegyi et al. (2005) focussed on VSL within second-order macroscopic traffic flow models, they emphasised the importance of validation to confirm the appropriateness of their proposed models since the impact of VSL on traffic behaviour is still not well understood (Hegyi et al. 2005; Papageorgiou et al. 2008). For CTM, the most commonly used method (Chiou et al. 2012; Hadiuzzaman and Qiu 2013; Li et al. 2015) is to assume that VSL operation influences the demand part of the FD i.e. the free-flow traffic speed (u_f) and maximum traffic flow (Q_{max}) parameters, as shown in **Fig. 1b**. The consequence is a reduction of outflows to downstream cells, reducing congestion levels. **Eq. 4** and **Eq. 5** are modified to give **Eq. 14** and **Eq. 15**, respectively. The VSL for cell *i* at time step *t,* $\tilde{u}_{VSL_i}(t)$ in km h^{-1}, needs to be obtained as input data, while the maximum traffic flow, $Q_{VSL_i}(t)$ in veh h^{-1} lane^{-1}, can be calculated from the FD (see **Fig. 1b**).

$$S_i(t) = min\{min[u_f, \tilde{u}_{VSL_i}(t)]\,\rho_i(t), min[Q_{max}, Q_{VSL_i}(t)]\}\lambda_i \quad \textbf{(14)}$$

$$R_{i+1}(t) = min\{w[\rho_{max} - \rho_{i+1}(t)], min[Q_{max}, Q_{VSL_{i+1}}(t)]\}\,\lambda_{i+1} \quad \textbf{(15)}$$

In reference to **Eq. 1**, *f = CTM-basic* refers to the CTM formulation for a non-VSL road network whereas *f = CTM-vsl* represents the CTM formulation for a VSL road network. To summarise, the model input data represents the initial traffic density condition, the traffic demand at origins (mainline and on-ramps), split ratios at off-ramps, and traffic density at the mainline destination. Under CTM-vsl, the speed limits for each cell and time step are additional inputs. The model parameter vector consists of the four FD parameters $\beta = (u_f, Q_{max}, w, \rho_{max})$, which need to be calibrated.

Given the traffic density per lane and traffic speed CTM model outputs, the average speed-based emission $E_i^a(t)$ of air pollutant *a* in grams produced in cell *i* during time step *t* can be calculated using **Eq. 16**. γ_c is the proportion of vehicle category *c* which denotes not only vehicle class (e.g.

passenger car) but also fuel type (e.g. diesel) and emission standard (e.g. Euro 5 for European vehicles). The emission factor in grams per distance travelled (typically in grams km^{-1}) for air pollutant *a* is $ef^{a,c}[u_i(t)]$, for vehicle category *c* and average speed $u_i(t)$. The first part of **Eq. 16** thus determines the total vehicle distance travelled in cell *i* during time step *t* required to calculate total grams produced.

$$E_i^a(t) = \sum_c \rho_i(t)\lambda_i l_i \gamma_c u_i(t) T_s ef^{a,c}[u_i(t)] \quad (\mathbf{16})$$

CTM is not inherently a multi-class model, ignoring differences amongst different vehicle classes. Emissions factors are considered only for vehicles subject to the National Speed Limits, namely Passenger Cars (PCs) and Light Duty Vehicles (LDVs); total vehicle distance is divided proportionately depending on different fuel types and vehicle standards, with all vehicles assumed to be of these two classes.

Different emissions models (and hence emissions factors) are typically developed for different countries, depending on relevant vehicle classes, fuel types, and emission standards. In this study, the COmputer Programme to Calculate Emissions from Road Transport (COPERT) emission factors (Ntziachristos et al. 2000) are used. Note that, as discussed below, the potential pitfalls of integrating high-resolution CTM with average speed-based emission models are quite general, and are not confined to the specific choice of COPERT.

The integrated traffic flow – exhaust emission modelling approach can be summarised in **Eq. 17** where the 2-D matrix E^a captures the space-time dynamics of emission predictions based on the CTM outputs and the above emission model (*EM*).

$$\begin{aligned} E^a &= EM\{\gamma, (\rho, u), ef^a(u)\} \\ &= EM\left\{\gamma, f\left(\tilde{I}, \beta(\tilde{Z})\right), ef^a\left[f\left(\tilde{I}, \beta(\tilde{Z})\right)\right]\right\} \end{aligned} \quad (\mathbf{17})$$

Sources of uncertainty in emission predictions can be identified based on the above modelling chain. These can be categorised into four:

- The emission model inputs which correspond to vehicle proportions and traffic data

input or, in this case, the CTM model outputs; these are used either directly or nested within the emission factor functions.

- The emission model parameterisation nested within the emission factor functions which are highly parameterised vehicle class/fuel type/standard-specific nonlinear functions of average speed.

- The emission model structure itself which relies on the assumption that macroscopic traffic behaviour in terms of average speed can predict emissions without consideration of individual driving behaviour. Nested within are the emission factor functions that also rely on point-based prediction of emissions per unit distance given a particular average speed, rather than probabilistic-based prediction.

- The integration of average speed-based emission models with continuum macroscopic traffic flow models with respect to three key aspects: the compatibility of the high spatial (very short links) and temporal (very short time intervals) resolution traffic flow model outputs with emission models typically developed based on lower traffic data resolution (see for e.g. Samaras et al. 2014); the compatibility of the averaging type of predicted traffic speed (link-based averages) with emission models typically developed based on trip-based averages of traffic speed (see for e.g. Bai et al. (2007) and Wismans et al. (2011) for a discussion); and the compatibility of a single-class traffic flow model with multi-class emission model formulation.

The above highlights key sources of uncertainty in the described modelling system. However, it is clear from **Eq. 17** that most recurring sources of uncertainty in emission predictions are the traffic flow model input data $\tilde{I}$, parameter vector β, and model structure f. Li et al. (2012) argued that input uncertainty can be controlled through better measurement techniques, but the parameter vector that specifies the FD is the essential and dominant source of uncertainty. This paper focusses on two interdependent sources of uncertainty: the parameter vector and the model structure of CTM. A

data-driven methodology to capturing and propagating uncertainty from these two sources to emission predictions is described in **section 2.2**.

2.2. Methodological framework

In order to quantify uncertainty in CTM-based emission predictions arising from uncertainty in CTM model parameters and structure, this paper develops a five-phase data-driven methodology comprising: road traffic data preparation; ensemble-based optimisation; error estimation; grid-based Monte Carlo sampling; and uncertainty propagation. **Fig. 2** provides a summary of the steps and key annotations for each of these five phases.

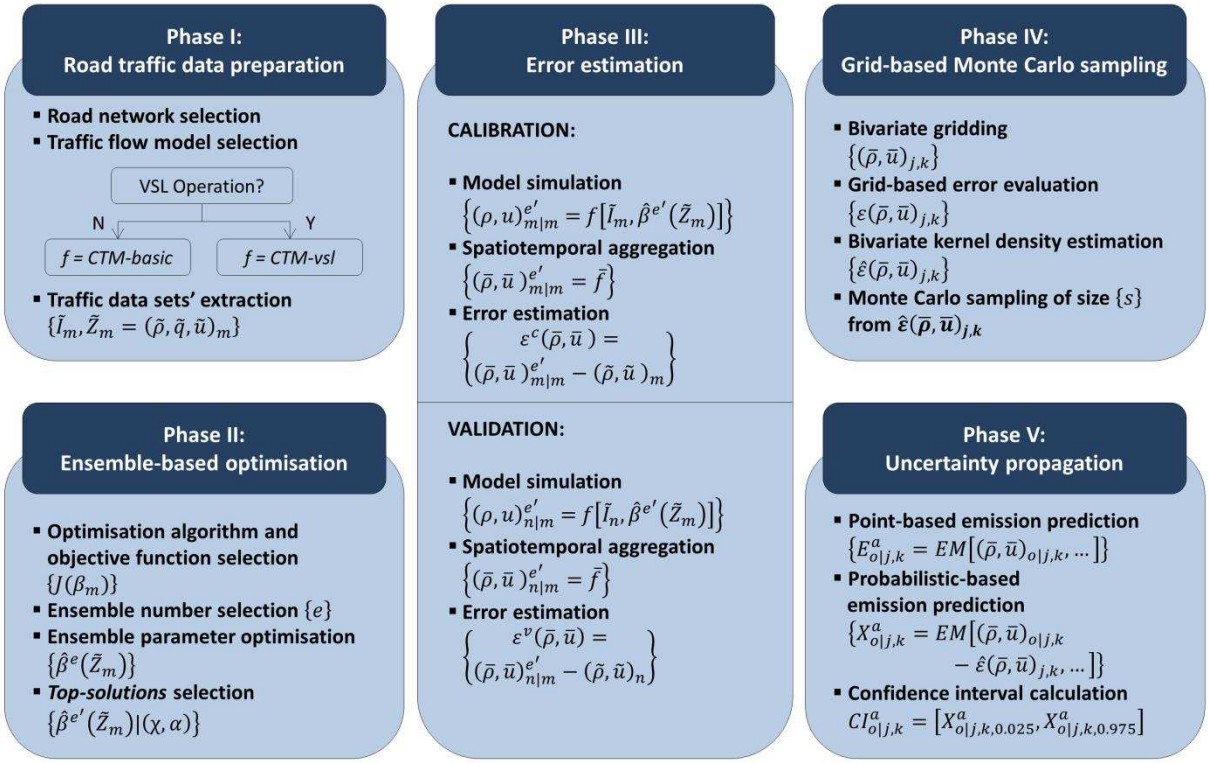

Fig. 2: five-phase data-driven methodological framework to uncertainty propagation from macroscopic traffic flow models to average speed-based exhaust emission predictions. [c and v] in Phases IV and V are dropped for convenience.

The first 'road traffic data preparation' phase follows directly from the description of CTM. This involves identification of a road network to be studied and selection of the appropriate CTM (with/without VSL), plus extraction of data required for CTM inputs and for the calibration of the CTM parameters. Let *M* denote the number of data sets for a specific road network such that,

$$\{\tilde{I}_m,\ \tilde{Z}_m = (\tilde{\rho}, \tilde{q}, \tilde{u})_m;\ m = 1,2,\dots,M;\ M > 1\}$$

where $(\tilde{\rho}, \tilde{q}, \tilde{u})_m$ are estimated traffic density, measured traffic flow, and measured traffic speed at all the measurement sites within the mainline boundaries of the network and throughout the entire period of data set *m*. Traffic density is typically not directly measured (e.g. by loop detector) but rather estimated based on flow and speed measurements.

For each data set *m*, the optimal parameter vector β_m needs to be determined. A number of derivative-free algorithms have been applied to similar problem (generally for macroscopic traffic flow model parameter estimation), such as the 'Genetic Algorithm' (Michalewicz 1994) in Poole and Kotsialos (2012), the 'cross-entropy' method in Ngoduy and Maher (2012), the 'Particle Swarm Algorithm' (Eberhart and Kennedy 1995) in Poole and Kotsialos (2016), and the 'Nelder-Mead' algorithm (Nelder and Mead 1965) in Spiliopoulou et al. (2014, 2015). It is notable that in most of these calibration and validation studies, only one (typically local) solution for a specific data set is determined, with this solution selected via a qualitative assessment of the model output against real data. Ni et al. (2004) proposed a systematic approach to the calibration of macroscopic traffic flow models and suggested the use of statistical inference to help select optimal parameters. In this paper, an ensemble-based optimisation approach is proposed to account for the uncertainty in the optimal parameter vector for a specific data set, followed by statistical inference to select *top-solutions* for a given data set *m*.

According to Cullen and Frey (1999), uncertainty in model parameters can result from input uncertainty or from model uncertainty if the structural form of the model is not adequate. This is referred to as systematic uncertainty (e.g. Frey and Burmaster 1999; Cullen and Frey 1999; and others). These two factors are relevant here, and additionally the parameter optimisation approach introduces uncertainty as a result of the nonlinearity and complexity of the problem, which typically does not find a unique optimal solution (even if one exists).

Uncertainty in a parameter vector can also arise from inherent variability for example due to the stochasticity of traffic behaviour. In other modelling frameworks, such uncertainty is typically

referred to as variability or stochastic uncertainty, which cannot be reduced (e.g. Frey and Burmaster 1999; Cullen and Frey 1999; and others). In this paper we do not attempt to address this type of uncertainty.

The second 'ensemble-based optimisation' phase begins with selection of an optimisation algorithm and objective function. Despite recognised deficiencies of the 'Nelder-Mead' algorithm in terms of its possibility of approximating a local optimum and its dependence on the initial parameter set, Spiliopoulou et al. (2015) showed that the algorithm is comparable to other methods such as GA when it is applied several times with different initial conditions, while being comparatively attractive in terms of its ease and of use and computational efficiency. In this paper, the unconstrained 'Nelder-Mead' algorithm (R Core Team 2015; Bihorel and Baudin 2015) has been used. The objective function is the sum of absolute errors of measured versus predicted traffic speed as shown in **Eq. 18** where $\widetilde{N}$ is the number of dual loop detectors (excluding the origin and destination ones); $\tilde{T}$ is the number of measurement time steps; $\tilde{u}_{\tilde{\imath}}(\tilde{t})$ is the measured traffic speed at loop detector $\tilde{\imath}$ and measurement time step $\tilde{t}$; and $\bar{u}_{\tilde{\imath}}(\tilde{t})$ is the space-time aggregate predicted traffic speed at loop detector $\tilde{\imath}$ and measurement time step $\tilde{t}$. $\widetilde{N}$ is used since origin and destination measurement data are utilised as model input (particularly as boundary conditions) and are hence excluded from the objective function. Since the temporal resolution of measured traffic speed is typically lower than that of predicted speed, the CTM speed output is time-averaged to match the resolution of real data. Spatially, only cells where real measurements exist are included in the objective function.

$$J(\beta_m) = \frac{1}{\widetilde{N}}\frac{1}{\tilde{T}}\sum_{\tilde{\imath}=1}^{\widetilde{N}}\sum_{\tilde{t}=1}^{\tilde{T}}[|\bar{u}_{\tilde{\imath}}(\tilde{t}) - \tilde{u}_{\tilde{\imath}}(\tilde{t})|_m] \quad \textbf{(18)}$$

Parameter vector β_m has to satisfy the two FD conditions and the Courant–Friedrichs–Lewy condition. Hence, three penalty terms are added to the optimisation algorithm. An ensemble-based approach entails running the algorithm multiple times, resulting in a set of optimal parameter vectors. Let *E* denote the number of optimisation runs, with $\hat{\beta}^e$ the optimal parameter vector obtained from run e, such that,

$$\left\{\hat{\beta}^e\left(\tilde{Z}_m\right) = argmin\, J(\beta_m^e); e = 1,2,\dots,E\right\}$$

Each run is initialised with a randomly sampled vector β^e within which each parameter is drawn from a predefined distribution. Some of these optimisation runs result in poor solutions, and so a quantitative statistical inference method is used to select those that are satisfactory. Let *E′* denote the number of *top-solutions* such that,

$$\{\hat{\beta}^{e'}(\tilde{Z}_m);\ e' = 1,2,\dots,E';E' < E\}$$

Top-solutions are optimal parameter vectors that capture both the distribution and variance of measured traffic data. Specifically, for each optimal parameter vector $\hat{\beta}^e$ the CTM is simulated and the time-averaged predicted traffic density and speed at measurement locations are obtained. Two statistical tests are applied to measured versus predicted traffic variables. These are: the non-parametric Mann-Whitney to test whether or not the distribution of the measured variable differs from that of the predicted variable by a location shift; and the non-parametric Fligner-Killeen to test whether or not the distributions' variances differ at a predefined significance level. A parameter vector $\hat{\beta}^e$ is selected if any of the following two conditions is satisfied:

- the objective function value lies within the minimum χ of all optimisation runs for a specific data set *m*, and both the distribution and variance of the measured and predicted *traffic density* are not different at significance level α.
- the objective function value lies within the minimum χ of all optimisation runs for a specific data set *m*, and both the distribution and the variance of the measured and predicted *traffic speed* are not different at significance level α.

Requiring that CTM outputs satisfy both conditions simultaneously turns out to be too demanding, given that CTM only captures the dynamics of traffic density and assumes steady-state speed-density conditions. By defining χ and α, only the *top-solutions* $\hat{\beta}^{e'}$ are considered for the next phase of analysis, 'error estimation'. When the CTM is run using *top-solutions* of data set *m* and input for data set *m*, this is referred to as a calibrated CTM model. However, when the CTM is run using *top-solutions* of data set *m* but using input data set n $\{n = 1,2,\dots,M-1;\ n \neq m\}$, this is referred to

as a validated CTM model. Given *top-solutions* $\hat{\beta}^{e'}$, let $(\rho, u)_{m|m}^{e'}$ and $(\rho, u)_{n|m}^{e'}$ denote the predicted traffic density and speed data at all cells $i\,\{i = 1,2, \dots N\}$ (i.e. excluding origin cell *0* and destination cell *N+1*) and all time steps $t\,\{t = 1,2, \dots, T\}$ for calibrated CTM models and validated CTM models, respectively, such that,

$$\left\{(\rho, u)_{m|m}^{e'} = f\left[\tilde{I}_m, \hat{\beta}^{e'}\left(\tilde{Z}_m\right)\right]\right\}$$

$$\left\{(\rho, u)_{n|m}^{e'} = f\left[\tilde{I}_n, \hat{\beta}^{e'}\left(\tilde{Z}_m\right)\right];\ n = 1,2, \dots, M-1;\ n \neq m\right\}$$

As a result of the different spatiotemporal resolution in comparison to real measurements, predicted data on cells where measurement sites exist are extracted (except for the origin and destination measurement sites for which the data has been used as CTM model input) and are time-averaged to match the temporal resolution of real data. Let $(\bar{\rho}, \bar{u})_{m|m}^{e'}$ and $(\bar{\rho}, \bar{u})_{n|m}^{e'}$ denote all the aggregated predicted traffic density and speed data required for the estimation of calibration and validation errors, respectively, such that,

$$\left\{(\bar{\rho}, \bar{u})_{m|m}^{e'} = \bar{f}\left[\tilde{I}_m, \hat{\beta}^{e'}\left(\tilde{Z}_m\right)\right]\right\}$$

$$\left\{(\bar{\rho}, \bar{u})_{n|m}^{e'} = \bar{f}\left[\tilde{I}_n, \hat{\beta}^{e'}\left(\tilde{Z}_m\right)\right]\right\}$$

For a particular road network, a bivariate traffic density and speed error distribution can be estimated for each of the calibration and validation CTM outputs separately. The estimated errors can be attributed to uncertainty in both the parameters and/or model structure (i.e. even if the global optimum parameter vector exists and is obtained, errors will still occur due to the model structure). Given the measured traffic density and speed $(\tilde{\rho}, \tilde{u})$, let these errors be denoted as $\varepsilon^c(\bar{u}, \bar{\rho})$ and $\varepsilon^v(\bar{u}, \bar{\rho})$ such that,

$$\left\{\varepsilon^c(\bar{\rho}, \bar{u}) = (\bar{\rho}, \bar{u})_{m|m}^{e'} - (\tilde{\rho}, \tilde{u})_m\right\}$$

$$\left\{\varepsilon^v(\bar{\rho}, \bar{u}) = (\bar{\rho}, \bar{u})_{n|m}^{e'} - (\tilde{\rho}, \tilde{u})_n\right\}$$

The distribution of errors varies across the feasible region of traffic densities and speeds; errors occurring at high speed free-flow conditions are systematically different from those associated with highly congested, low speed conditions. In principle, a bivariate error distribution of traffic density and speed could be associated with each density-speed point, but estimating this would require incredibly high data density throughout the feasible region. A grid-based approach is therefore used. Let $(\bar{\rho}, \bar{u})_{j,k}\ \{j = 1,2, \dots, J; k = 1,2, \dots, K\}$ define the $[j, k]$ grid square of the predicted density-speed region. The bivariate error distribution for each grid square can be determined and is annotated as $\varepsilon(\bar{\rho}, \bar{u})_{j,k}$. A bivariate kernel density $\hat{\varepsilon}(\bar{\rho}, \bar{u})_{j,k}$ can then be estimated for each grid square from which a Monte Carlo random sample with size s can be generated and associated with the corresponding gridded bivariate predicted density-speed region. This is the fourth 'grid-based Monte Carlo sampling' phase of the methodological framework, and is applied separately to the calibration and validation errors.

By capturing the bivariate error distribution for each predicted traffic density and speed grid square, uncertainty in the CTM outputs can be quantified and propagated to emission predictions: the final 'uncertainty propagation' phase. Let $E^{a}_{o|j,k}$ denote the predicted emissions for air pollutant *a* evaluated at a density-speed point, *o*, within the $[j, k]$ grid square,

$$\left\{E^{a}_{o|j,k} = EM\left[(\bar{\rho}, \bar{u})_{o|j,k}, \dots\right];\ o \in [j, k];\ j = 1,2, \dots, J;\ k = 1,2, \dots, K\right\}$$

The uncertainty of each predicted density-speed point can be quantified by adding the sampled error of the same grid square. Given the bivariate error distribution associated with the $[j, k]$ grid square, let $X^{a}_{o|j,k}$ denote the distribution of emission predictions at the density-speed point, *o*, in $[j, k]$ grid square such that,

$$\left\{X^{a}_{o|j,k} = EM\left[(\bar{\rho}, \bar{u})_{o|j,k} - \hat{\varepsilon}(\bar{\rho}, \bar{u})_{j,k}, \dots\right]\right\}$$

The 2.5th and 97.5th quantile of the distribution $\{X^{a}_{o|j,k,0.025}, X^{a}_{o|j,k,0.975}\}$ provide the lower and upper bounds of the emission prediction at the density-speed point at a 95% confidence level. The selected sample size *s* determines the precision of the calculated quantiles (Morgan et al. 1992); to

be 95% confident that the actual 97.5th (or 2.5th) quantile is between the estimates of 96.5th and 98.5th (or 1.5th and 3.5th) quantiles, a sample size $s = 1000$ was found to be sufficient. Evaluating the lower and upper bounds at equally spaced density-speed prediction points in each grid square provides a surface map of the confidence interval of emission predictions of pollutant a throughout the entire prediction region. By using the calibration and validation predictions and their corresponding estimated error distributions separately, a surface map of confidence intervals can be deduced for each.

3. Study sites and data collection

Unlike most previous studies, this paper considers multiple real road networks and data sets from multiple days in order to thoroughly test the proposed methodology and ensure transferability of findings. The paper also considers both a VSL and non-VSL operated road networks in order to investigate how both the CTM-basic and CTM-vsl perform under real-world scenarios especially that calibration and validation studies of the CTM-vsl are limited to date despite the widespread operation of VSL across the UK road network and worldwide.

Three motorway routes have been selected, each with different characteristics. These are a 3.1 km route on the non-VSL M60 motorway, a 3.8 km route on the non-VSL M1 motorway, and a 4.8 km route on the VSL M25 motorway. Each route is equipped with a number of dual loop detectors as part of the Motorway Incident Detection and Automatic Signalling (MIDAS) network (MIDAS 2016). **Fig. 3** shows the selected routes and geographic locations of dual loop detectors on each of the three routes and **Table 1** provides detailed description of the road network characteristics and traffic data set characteristics for each selected routes. The identification of road network characteristics and the preparation of the traffic data sets are considered the first phase of the proposed methodological framework.

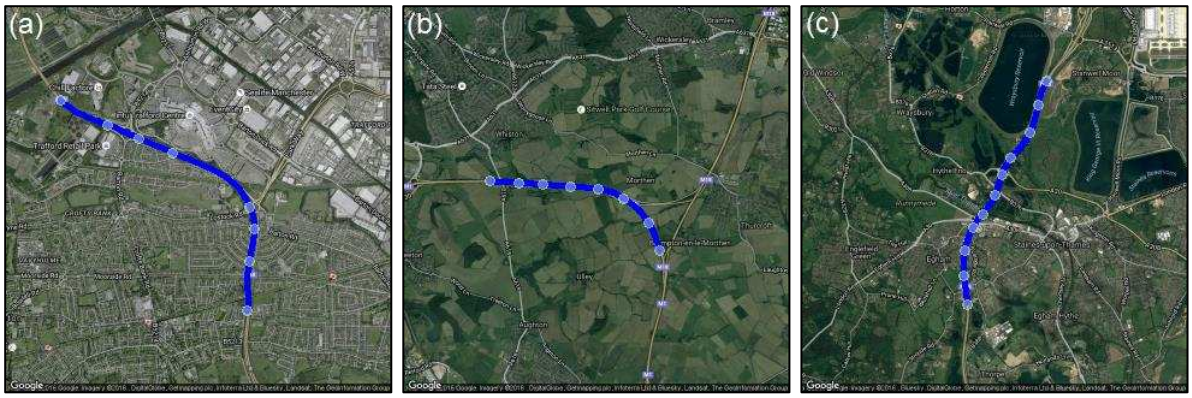

Fig. 3: Map location of the three selected road networks: (a) non-VSL M60, (b) non-VSL M1, and (c) VSL M25 represented by the dark blue coloured line; light blue coloured circles indicate the location of dual loop detectors available along each route under study excluding the on-ramps and off-ramps dual loop detectors. All figures in this paper are plotted using the R project for Statistical Computing (R Core Team 2015), particularly, RgoogleMaps and Loa packages (Loecher and Ropkins 2015) and Lattice package (Sarkar 2008).

The first M60 route is located on the western side of the Manchester Ring Motorway between J8 and J11. Encircling Greater Manchester and with two on-ramps and two off-ramps located along the route, this section is characterised by its recurrent congestion specifically during the AM and PM peak periods with a two-way annual average daily traffic on J11 reported to reach 138,000 vehicles per day during 2013 (Department for Transport 2016). 8 dual loop detectors are located on the M60 route with additional 4 dual loop detectors located on each off-ramp and on-ramp. Based on the route configuration and the loop detector locations, the route has been divided into 15 cells (excluding the mainline origin and destination segments) with lengths varying between 0.1 km and 0.285 km. So, the calibration problem will include data of 6 loop detectors located at 6 cells out of 15.

The second route is located on the northern end of the M1 motorway between J31 and J33 near Sheffield City. The M1 motorway is considered to be a major connection between London and northern UK and thus is also characterised by recurrent congestion during the AM and PM peak periods with a two-way annual average daily traffic on J31 reported to reach 126,000 vehicles per day during 2013 (Department for Transport 2016). 8 loop detectors are located on the M1 route with additional loop detector on an on-ramp. The route has been divided into 13 cells (excluding the mainline origin and destination segments) with lengths varying between 0.22 km and 0.33 km. The calibration problem involves data from 6 detectors at 6 cells out of 13.

The third route is located on the western side of the London Orbital Motorway between J14 and J12. Encircling greater London, the M25 motorway is one of the busiest motorways in the UK with a two-way annual average daily traffic on J14 reported to reach 228,000 vehicles per day during 2013 (Department for Transport 2016). Unlike the first two routes, this route is considered a controlled motorway section and thus operates VSL. Enforced speed limits on the M25 motorway route can vary by loop detector location, motorway lane, and time period typically between 40 miles per hour (or 65 km h^{-1}) and 60 miles per hour (or 96 km h^{-1}). In the absence of VSL signs, the motorway speed limit is assumed to be 70 miles per hour (or 113 km h^{-1}). 11 loop detectors are located on this route with additional 2 loop detectors located on an off-ramp and on-ramp along the route. Between the off-ramp and on-ramp, the number of lanes drops from 5-lanes to 4-lanes, unlike the first two routes which are 3-lane sections throughout. This route has been divided into 18 cells (excluding the mainline origin and destination segments) with lengths varying between 0.14 km and 0.38 km. The calibration will include 9 loop detectors at 9 cells out of 18. **Table 1** provides a detailed summary of the road network characteristics of each of the three selected routes.

Table 1: summary of the non-VSL M60, non-VSL M1, and VSL M25 road network characteristics and traffic data set characteristics

Study site		**M60**	**M1**	**M25**
Road network characteristics	**Route location**	Manchester Orbital	Sheffield City	London Orbital
	Route direction	Northbound	Northbound	Anti-clockwise
	Route length [km]	3.1	3.8	4.8
	Start point OS grid reference	[377526, 394773]	[448017, 388049]	[503129, 174537]
	End point OS grid reference	[375778, 396773]	[444800, 389325]	[501650, 170116]
	Variable Speed Limit (VSL) operation	No	No	Yes
	Nr. of cells (*N*)[1]	15	13	18
	Nr. of lanes per cell	3	3	5 and 4
	[min, max] cell lengths [km]	[0.1, 0.285]	[0.22, 0.33]	[0.14, 0.38]
	Nr. of loop detector-cells[2]	6	6	9
	Nr. of non-loop detector-cells	9	7	9
	Nr. of on-ramp(s)	2	1	1
	Nr. of off-ramp(s)	2	0	1
Traffic data characteristics	**Data source**	Motorway Incident Detection and Automatic Signalling (MIDAS)		
	Data time resolution	1-minute	1-minute	1-minute
	Nr. of data sets (*M*)	6	6	6
	Selected model (*f*)	CTM-basic	CTM-basic	CTM-vsl CTM-basic
	Date of data sets [mm-yyyy]	04-2013	06/07-2013	05-2014

	Nr. of AM period data sets	0	6	3
	Nr. of PM period data sets	6	0	3
	Time period per data set [h]	[6, 6, 6, 6, 3, 3]	[3, 3, 3, 3, 5, 4]	[3, 3, 3, 3, 5, 5]

[1]The number excludes mainline origin cell *0* and destination cell *N+1*.

[2]Loop detectors are located at the end of each loop detector-cell consistently for all the three routes. The number excludes mainline origin and destination dual loop detectors (which exist and are used to extract required input of traffic flow models) and excludes on-ramp(s) and off-ramp(s) loop detectors. There exist a loop detector on each on-ramp and off-ramp of each route. While MIDAS loop detectors are often referred to as being equally spaced (500 meters), this is not necessarily the case in reality, spacing ranges between 200 meters to 930 meters in this study. Spatial coordinates of loop detectors are extracted from the MIDAS coordinates data base and cross checked with Google Earth surface level view. Google Earth surface level location of dual loop detectors is considered the reference in this study.

For each of the selected routes, six data sets (i.e. $M = 6$) have been extracted from the MIDAS database (MIDAS 2016) in order to estimate both the calibration and validation errors of the traffic flow model at each route. The time period of each data set ranges between 3 and 6 hours and typically includes the AM peak period or the PM peak period. Details on the selected traffic data sets are provided in **Table 1**. The extracted data includes 1-minute traffic flow and traffic speed at each lane from each dual loop detector located along each of the three routes. Some data transformations were needed to prepare the input data for the model calibration. First, average traffic flow and weighted average traffic speed across all lanes are calculated according to Treiber and Kesting (2012); weighted average traffic speed is assumed to be an approximation of space-mean traffic speed. Average traffic density is then estimated using the traffic flow-density relationship. Additionally, off-ramp split ratios are calculated as the ratio of the measured off-ramp traffic flow to the total measured traffic flow. The latter is defined as the mainline traffic flow measured downstream an off-ramp plus the off-ramp traffic flow (Muñoz et al. 2004). The resulting traffic density, flow, and speed matrices provide the initial and boundary conditions needed for the CTM and the loop detector data needed for the ensemble-based optimisation as explained in **section 2.2**. Particularly, traffic flow measurements at the first loop detector which is allocated to mainline origin cell *0* are used as the traffic demand input to CTM; traffic density measurements at the last loop detector which is allocated to mainline destination *N+1* are used as a boundary condition at destination; and measurements from loop detectors in between the origin and destination are used for the ensemble-based optimisation phase. Since traffic outflow from mainline origin is restricted by the receiving capacity of cell *1* and since traffic density at mainline destination is imposed to model

the backward wave propagation of congestion, traffic conditions at origin and destination need not be congestion-free. For the input data to match the spatial (number of segments higher than the number of loop detectors for all routes) and temporal (T_s *= 2* seconds for the M60 and T_s *= 3* seconds for M1 and M25) resolution of CTM, data is interpolated where necessary.

The M60 and M1 traffic data sets are from 2013 at which time these routes did not operate VSL. Accordingly, the CTM-basic model, described in **section 2.1**, is used for calibration and validation. Given the operation of the VSL on the selected M25 route, the CTM-vsl model is used for calibration and validation. For comparison, the CTM-basic model was also run for the M25 data. The VSL data for the M25 route has been extracted from the Highways England databases for the relevant days. The final four modelling scenarios are:

- *M60/CTM-basic*: $\{f_{M60}[\tilde{I}_m, \beta(\tilde{Z}_m)];\ m = 1,2,\dots,6\}$
- *M1/CTM-basic*: $\{f_{M1}[\tilde{I}_m, \beta(\tilde{Z}_m)];\ m = 1,2,\dots,6\}$
- *M25/CTM-vsl*: $\{f_{M25}[\tilde{I}_m, \tilde{u}_{VSL}, \beta(\tilde{Z}_m)];\ m = 1,2,\dots,6\}$
- *M25/CTM-basic*: $\{f_{M25}[\tilde{I}_m, \beta(\tilde{Z}_m)];\ m = 1,2,\dots,6\}$

4. Results and discussion

Given road traffic data, the next four phases of the described methodological framework (**Fig. 2**) have been applied based on each of the four modelling scenarios. The optimisation approach is set out in **section 2.2**. The first step is to run the algorithm *e* times, with different initial model parameters, and record the final parameter vectors, $\hat{\beta}^e(\tilde{Z}_m)$, and minimised objective function values, $J(\hat{\beta}_m^e)$. In this study, *e* has been set to 500 for each data set of each modelling scenario. **Fig. 4** shows the optimisation results.

To identify the *top-solutions* $\hat{\beta}^{e'}(\tilde{Z}_m)$ for the four scenarios, two parameters are needed: the threshold quantile for objective function values is set to be χ *= 50%*; and the significance level for the two statistical tests is set to be α *= 0.01*. Using these values, **Fig. 4** shows the objective function values of the *top-solutions* (highlighted in dark blue circles). A total of 392 and 1199 are obtained for

the M60/CTM-basic and M1/CTM-basic. For the M25, the CTM-basic resulted in 209 *top-solutions* compared with only 163 under the CTM-vsl; *top-solutions* being obtained for 5 data sets (out of 6) under the CTM-basic formulation but for only 2 data sets under the CTM-vsl. This suggests that the CTM-vsl may sometimes be problematic and may not necessarily be appropriate to describe traffic behaviour for all time periods especially when VSL operation changes by time, loop detector, and by lane as it does for this route. CTM-vsl assumes a uniform impact of VSL on traffic behaviour while this might not be necessarily true. For instance, compliance to different speed limits on different lanes and different sections during different time periods might not be necessarily the same. That said, the number of *top-solutions* for the *CTM-basic* drops to 11 (for a single data set only) when the significance level is set to 0.1 instead of 0.01; since this high drop does not happen for the M60 and M1 road networks, this indicates that also *CTM-basic* may be problematic for VSL-operated road networks.

Fig. 4 also shows that *top-solutions* were not identified for all data sets. Given the population of initial conditions tested in each case and the fact that 'Nelder-Mead' optimisation algorithm is a proven and reliable way to find a 'good' solution if one exists, this can be attributed to the CTM itself being unable to accurately reproduce all features of observed traffic data or at least features of observed traffic data that allows to meet the statistical inference criteria. This can be a result of deficiencies such as the use of simplified FD, use of steady-state speed-density relationship, and ignored influence of different vehicles classes, lane drops, and lane changing.

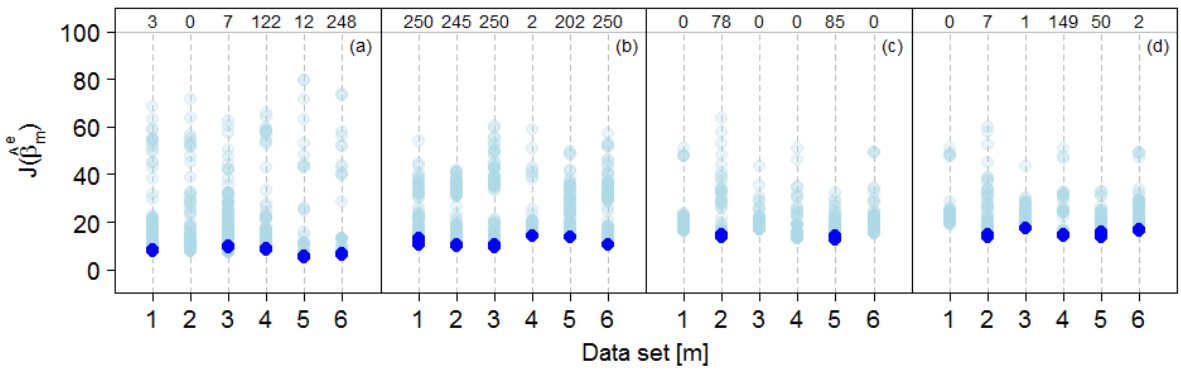

Fig. 4: minimised objective function values obtained from the *calibration* runs of (a) M60/CTM-basic, (b) M1/CTM-basic, (c) M25/CTM-vsl, and (c) M25/CTM-basic for each of the six selected data sets. Dark blue

coloured circles highlight the objective function values of the *top-solutions* (the number of *top-solutions* for each data set is highlighted on top of each figure) based on the defined statistical inference criteria (E' = 392, 1199, 163, and 209 for (a) M60/CTM-basic, (b) M1/CTM-basic, (c) M25/CTM-vsl, and (d) M25/CTM-basic is identified, respectivaly). One calibration run for (c) M25/CTM-vsl and one for (d) M25/CTM-basic did not converge based on the predefined convergence criteria and thus not shown here.

Table 2 shows the relative standard deviation (coefficient of variation) of each parameter based on identified *top-solutions* only. Lowest variability is observed in the demand parameters (i.e. the free-flow traffic speed and maximum traffic flow) and high variability is observed in the supply parameters (i.e. backward wave speed and jam traffic density). This emphasises the complexity of driving behaviour during congested periods and the possibility of the supply part to take different values under the CTM assumption of a trapezoidal FD. **Table 3** shows the range of parameter values for each modelling scenario irrespective of data set *m*. Note that parameter covariance may be positive or negative, and hence not independent. For instance, the lowest value of maximum traffic density for the M60/CTM-basic (83.5 veh km^{-1} $lane^{-1}$) was accommodated by high backward wave speed (45.7 km h^{-1}). Also, the highest value of maximum traffic density for the M1/CTM-basic obtained (504.3 veh km^{-1} $lane^{-1}$) was accommodated by very low backward wave speed (3.7 km h^{-1}). While such extreme cases rarely occur in the *top-solutions*, they cannot be entirely ignored as they replicate certain features of measured traffic conditions given a certain significance level. It is also essential to account for covariance when considering the sensitivity of CTM to perturbation in parameter values. **Appendix A** shows detailed results (in figures) of *top-solutions'* parameter values.

Table 2: coefficient of variation (%) of each parameter based on the *top-solutions* of all data sets of each of the M60/CTM-basic, M1/CTM-basic, M25/CTM-vsl, and M25/CTM-basic

CTM Parameter	M60/CTM-basic	M1/CTM-basic	M25/CTM-vsl	M25/CTM-basic
Free-flow traffic speed (u_f)	0.6%	0.6%	0.4%	0.7%
Maximum traffic flow (Q_{max})	10.3%	4.3%	3.2%	2.3%
Backward wave speed (w)	26.6%	24.2%	26.6%	26.3%
Maximum traffic density (ρ_{max})	15.9%	28.1%	23.6%	20.6%

Table 3: range [min, max] of each parameter based on the *top-solutions* of all data sets of each of the M60/CTM-basic, M1/CTM-basic, M25/CTM-vsl, and M25/CTM-basic

CTM Parameter	M60/CTM-basic	M1/CTM-basic	M25/CTM-vsl	M25/CTM-basic
Free-flow traffic speed (u_f)	[101, 105]	[104, 111]	[102, 105]	[100, 106]
Maximum traffic flow (Q_{max})	[1981, 2853]	[1719, 2048]	[1635, 1893]	[1601, 1797]
Backward wave speed (w)	[21.1, 51.1]	[3.7, 28.6]	[13.9, 41.2]	[10.3, 42.9]
Maximum traffic density (ρ_{max})	[83.5, 139.1]	[87.1, 504.3]	[60.1, 142.4]	[59.8, 178.4]

The *top-solutions* for each data set are then validated against all other data sets within the same road network. Validation results are shown in **Fig. 5**. Unsurprisingly, results show higher objective function values in comparison to those obtained from the calibration data which are annotated in dark blue in **Fig. 5**. Simulating the *top-solutions* on both calibration and validation data sets brings us to the third phase of the methodology which involves estimating the calibration and validation errors.

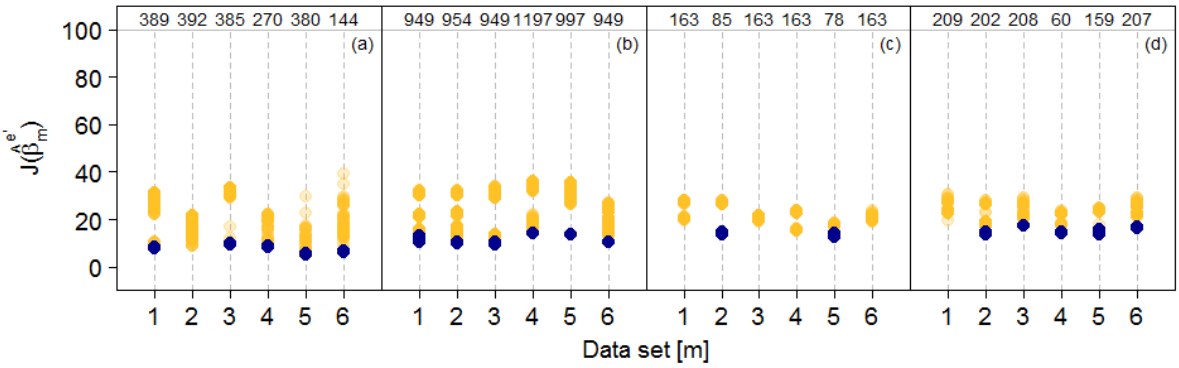

Fig. 5: objective function values obtained from the *validation* runs of the *top-solutions*, which are highlighted in dark blue coloured circles, for each of the six data sets of (a) M60/CTM-basic, (b) M1/CTM-basic, (c) M25/CTM-vsl, and (d) M25/CTM-basic on the remaining data sets of the same route. Total number of validation runs for each data set is highlighted on top.

Fig. 6 and **Fig. 7** present the error distributions obtained from the simulation of *top-solutions* on the calibration and validation data sets, respectively. The high resolution CTM outputs have been aggregated to 1-minute at loop-detector cells in order to calculate the errors in traffic density and speed. The figures show the bivariate error distributions $\varepsilon^c(\bar{\rho}, \bar{u})$ and $\varepsilon^v(\bar{\rho}, \bar{u})$ for each road network. For instance, *[3, 0, 7, 122, 12, 248] top-solutions* (total of *392*) have been identified for each of the six data sets of M60/CTM-basic modelling scenario. **Fig. 6a** shows the estimated calibration errors from all *392* simulations with a total of *568272* density-speed error points. Validation errors are computed by simulating the *top-solutions* of one data set using input data from the other five data sets. **Fig. 7a** shows the estimated validation errors from all the *1960* simulations (*392x5*) with a total of *3679440* density-speed error points.

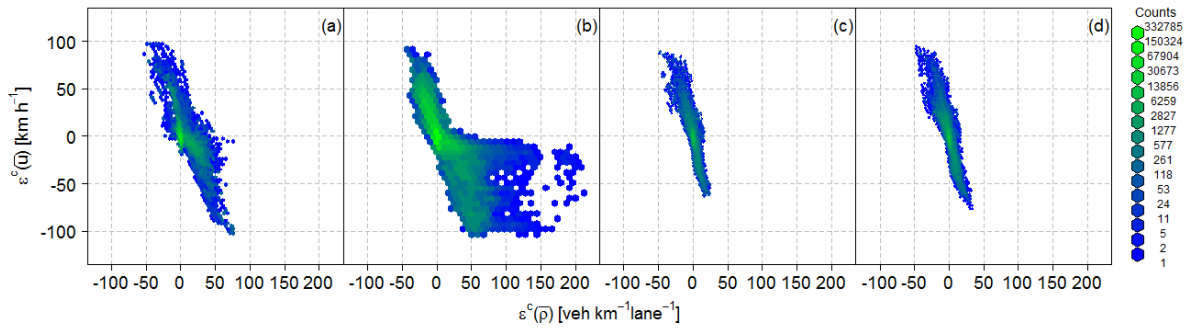

Fig. 6: bivariate error (ε) distributions of spatiotemporally-aggregated traffic density [veh km^{-1} lane^{-1}] and traffic speed [km h^{-1}] obtained from the simulation of the *top-solutions* on the *calibration* data sets of (a) M60/CTM-basic, (b) M1/CTM-basic, (c) M25/CTM-vsl, and (d) M25/CTM-basic with a total of 392, 1199, 163, and 209 simulations and total of 568272, 1537554, 357327, and 396621 density-speed error points, respectively.

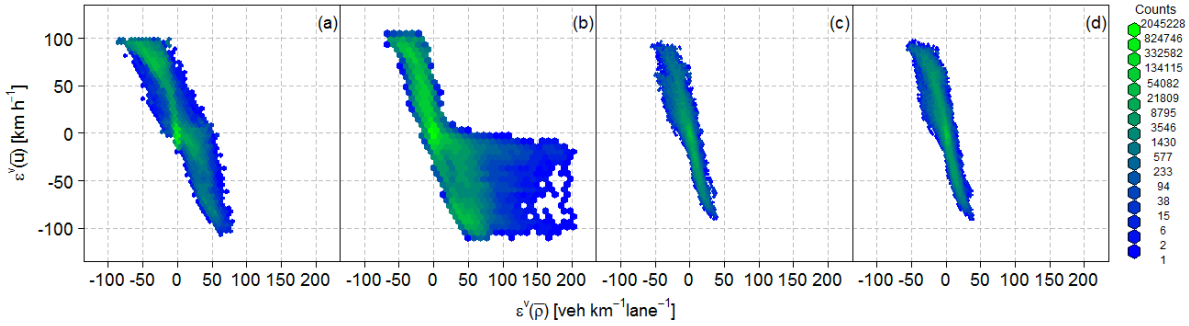

Fig. 7: bivariate error (ε) distributions of spatiotemporally-aggregated traffic density [veh km^{-1} lane^{-1}] and traffic speed [km h^{-1}] obtained from the simulation of the *top-solutions* on the *validation* data sets of (a) M60/CTM-basic, (b) M1/CTM-basic, (c) M25/CTM-vsl, and (d) M25/CTM-basic with a total of 1960, 5995, 815, and 1045 simulations and total of 3679440, 7570050, 1587915, and 2097585 density-speed error points, respectively.

The negative correlation clearly shows that an over prediction of traffic speed indicates an under prediction of traffic density and vice versa; a consequence of the FD speed-density relationship. The range of validation errors in traffic density and speed is higher than that of the calibration errors by a factor of 1.2 and 1.1, respectively, on average across all four modelling scenarios, as shown in **Table 4**, with higher variability. Also, while the number of *top-solutions* is lower for *CTM-vsl* in comparison with CTM-basic on the M25, the range and distribution of the final errors are very similar as shown in **Table 4**.

While these bivariate error distributions have been obtained from the simulation of *top-solutions* only, large calibration errors can occur e.g. a maximum over-prediction (under-prediction) of 76 (52) veh km^{-1} lane^{-1} and over-prediction (under-prediction) of 98 (102) km h^{-1} for M60/CTM-basic. Such

high error values, particularly of traffic speed, can be a direct result of the assumed steady-state speed-density relationship of CTM, i.e. average traffic speed adapting instantaneously to traffic density (Hoogendoorn and Bovy 2001).

Table 4: summary statistics (range, mean, and standard deviation) of traffic density [veh km^{-1} lane^{-1}] and traffic speed [km h^{-1}] errors shown in Fig. 6 and Fig. 7 for the *calibration* and *validation* runs, respectively

Statistic		M60/CTM-basic	M1/CTM-basic	M25/CTM-vsl	M25/CTM-basic
$\varepsilon^c(\bar{\rho},\bar{u})$	Range [min,max]	[-52,76], [-102,98]	[-44,213], [-103,91]	[-49,24], [-63,89]	[-48,33], [-76,96]
	Mean	(3.5, -0.7)	(1.3, 2.9)	(0.6, -0.5)	(0.5, -0.4)
	Std. Dev.	(10.5, 13.4)	(13.4, 18.8)	(7.1, 20.4)	(7.4, 20.4)
$\varepsilon^v(\bar{\rho},\bar{u})$	Range [min,max]	[-86,79], [-106,100]	[-67,202], [-110,105]	[-55,38], [-90,97]	[-56,38], [-90,97]
	Mean	(-6.7, 16.9)	(-0.3, 6.9)	(0.04, -1.5)	(-2.0, 7.5)
	Std. Dev.	(18.1, 34.7)	(18.3, 35.7)	(10.6, 29.0)	(11.0, 32.4)

As described in **section 2.2**, the error distributions illustrated in **Fig. 6** and **Fig. 7** are not uniformly populated by data across the range of densities-speeds (i.e. it would be inappropriate to associate the entire bivariate error distribution with every predicted point). Therefore a grid-based approach is undertaken. **Fig. 8** and **Fig. 9** show the gridding of predicted traffic density and speed based on *[J,K] = [15,15]* (i.e. 15 bins in each direction). **Appendix B** shows the results of a sensitivity analysis performed based on two other gridding criteria: *[J,K] = [10,10]* and *[J,K] = [20,20]*. The predicted density and speed points correspond to the *top-solutions* with the calibration data sets (**Fig. 8**) and validation data sets (**Fig. 9**). In this way, a bivariate error distribution for each grid square is identified and associated with the corresponding predicted density and speed points of the same grid square.

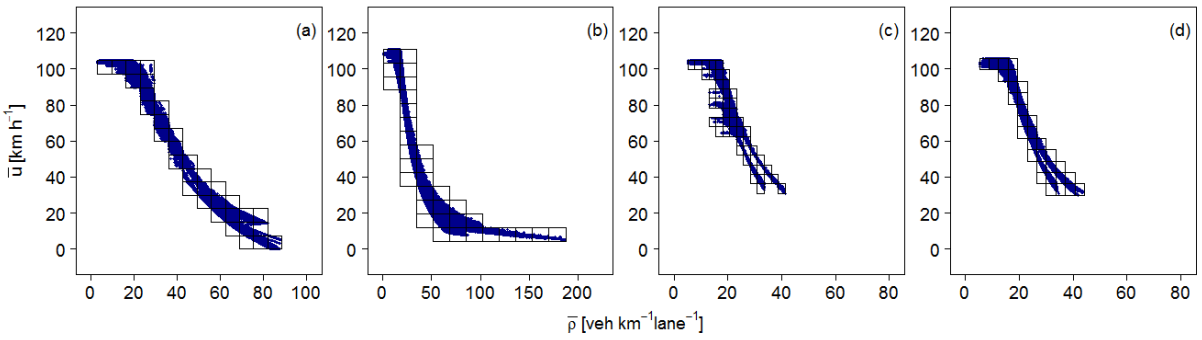

Fig. 8: modelled traffic density [veh km^{-1} lane^{-1}] and traffic speed [km h^{-1}] scatterplots obtained from the simulation of the *top-solutions* on the *calibration* data sets of (a) M60/CTM-basic, (b) M1/CTM-basic, (c) M25/CTM-vsl, and (d) M25/CTM-basic. Black squares show the 15x15 grid squares. Grid squares with data points less than 100 are not considered/removed.

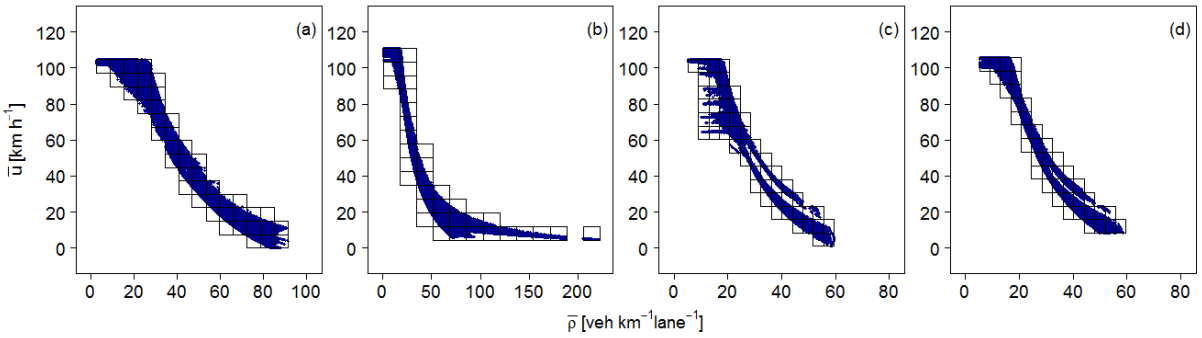

Fig. 9: modelled traffic density [veh km^{-1} lane^{-1}] and traffic speed [km h^{-1}] scatterplots obtained from the simulation of the *top-solutions* on the *validaiton* data sets of (a) M60/CTM-basic, (b) M1/CTM-basic, (c) M25/CTM-vsl, and (d) M25/CTM-basic.

The final phase is propagation of the bivariate errors to emission predictions. First, emissions of Oxides of Nitrogen (NO_x) are predicted in grams produced on one kilometre cell length during one minute time step at each feasible point in each density-speed grid square based on the COPERT average speed-based emission model, as described in **section 2.1** (**Eq. 16**). The one kilometre assumption is considered since errors here are considered collectively irrespective of space (i.e. cell). Results are shown in the top row of **Fig. 10** for each of the four scenarios. The vehicle proportions in each case have been obtained from DEFRA (2014). As discussed earlier, the CTM does not accommodate multi-class traffic flow and thus cannot be used to represent HGVs. It is therefore assumed that traffic comprises only PCs and LDVs with different fuel types and Euro standards that are typically allowed to drive up to the 70 miles per hour (i.e. 113 km h^{-1}) maximum speed limit. Based on random sampling size of *s = 1000*, the upper and lower bounds at each point of each grid square is calculated at a 95% confidence level. The results are shown in **Fig. 10** and **Fig. 11** based on the captured calibration and validation errors, respectively.

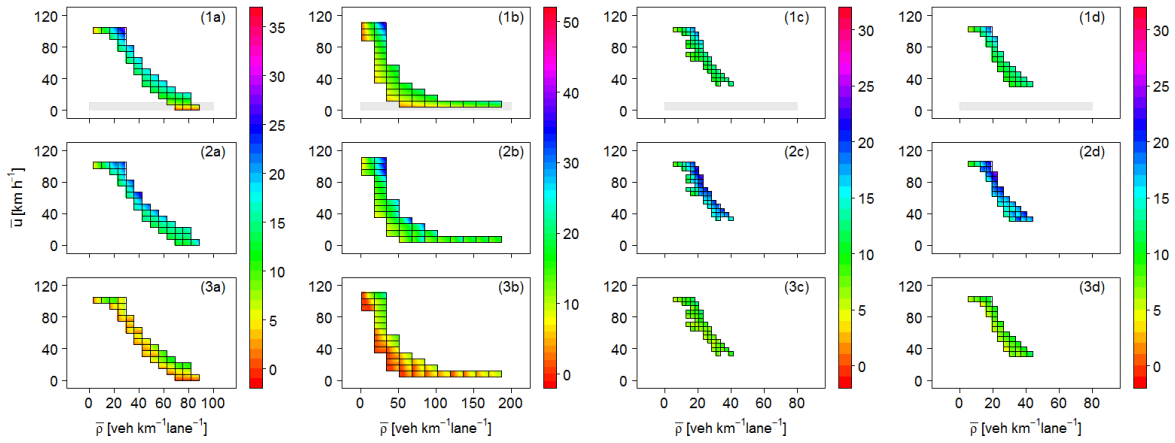

Fig. 10: Coloured contours showing NO_x emission predictions in grams produced in one kilometre space and one minute time as a function of modelled traffic density [veh km^{-1} lane^{-1}] and traffic speed [km hr^{-1}] using COPERT emission factors for PCs and LDVs (with different fuel type and Euro standard). Black lines show the grid squares. (1) Emission predictions based on *top-solutions* of the *calibration* data sets of (a) M60/CTM-basic, (b) M1/CTM-basic, (c) M25/CTM-vsl, and (d) M25/CTM-basic. Light grey rectangles in (1) represent uncertain emission predictions due to COPERT being restricted to >5 km h^{-1} or >10 km h^{-1} depending on vehicle class. Upper (2) and lower (3) bounds of emission predictions at a 95% confidence level based on error distributions obtained from the simulation of the *top-solutions* on the *calibration* data sets.

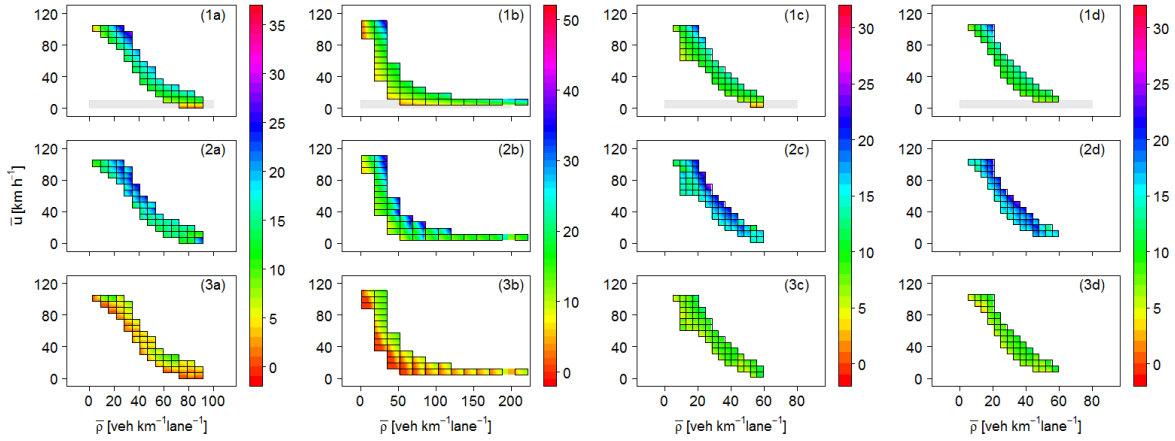

Fig. 11: Coloured contours showing NO_x emission predictions in grams produced in one kilometre space and one minute time as a function of modelled traffic density [veh km^{-1} lane^{-1}] and traffic speed [km hr^{-1}] using COPERT. (1) Emission predictions based on *top-solutions* of the *validation* data sets of (a) M60/CTM-basic, (b) M1/CTM-basic, (c) M25/CTM-vsl, and (d) M25/CTM-basic. Upper (2) and lower (3) bounds of emission predictions at a 95% confidence level based on error distributions obtained from the simulation of the *top-solutions* on the *validation* data sets.

Fig. 10 and **Fig. 11** allow examining not only the CTM-based emission predictions but also the interval of confidence in these emission predictions based on quantified uncertainties in the CTM calibration and validation model outputs, respectively. The difference between the upper (lower) bounds and the actual emission predictions are calculated in order to better understand the absolute uncertainty in emission predictions. **Table 5** describes the distribution of the additive upper (lower) bounds with respect to the actual emission predictions. As a sensitivity analysis, **Appendix B** shows

the results based on three gridding criteria: *[J,K] = [10,10], [15,15], and [20,20]*. Here, results based on *[J,K] = [15,15]* are presented in details. The analysis shows that while the distribution of additive upper bounds on errors does not change significantly based on the these three gridding choices, the range can be higher for lower grid square values and reduces with an increased grid square value up to a point at which the range of additive upper bounds ceases to decrease. In the modelling scenarios of this paper, it was found that at *[J,K] ≥ [15,15]*, the range of additive upper bounds ceased to decrease. Nevertheless, as the choice of the grid squares increases, the number of points within each grid square decreases which can influence the estimation of the bivariate kernel density of each grid square. So a trade-off between data occupancy and accuracy needs to be considered.

Based on estimated calibration errors, the mean additive upper bound for each modelling scenario is 1.9, 3.5, 4.5, and 5.0 grams produced in one kilometre space and one minute time while the mean additive lower bound is -8.8, -7.3, -3.8, and -4.4 grams. Based on estimated validation errors, however, the mean additive upper bound for each modelling scenario is 2.4, 4.5, 5.7, and 5.9 grams produced in one kilometre space and one minute time while the additive lower bound is -9.7, -7.9, -2.6, and -3.7 grams. This shows that the mean additive upper bounds based on estimated validation errors are consistently higher to those based on estimated calibration errors by a factor of 1.25 on average while the additive lower bounds are not necessarily higher for all modelling scenarios. Such differences can be attributable directly to the different estimated validation errors in comparison to the calibration ones plus to the fact that the validation prediction data occupy a wider traffic density and speed region as a result of the increased number of simulations and data points. Nevertheless, given the nonlinearity of the emission factors used and the different error distributions associated with different density-speed points, the higher validation errors does not necessarily imply higher additive lower bounds but rather depends on the error distributions and the quantified uncertainty in CTM model outputs (or emission model inputs).

Table 5: summary statistics of additive upper ($X_{0.975}$) and lower ($X_{0.025}$) bounds distributions in comparison to actual NO_x emission predictions (in grams produced in one kilometre space and one minute time) of calibration and validation data sets shown in Fig. 10 and Fig. 11, respectively

Statistic	M60/CTM-basic		M1/CTM-basic		M25/CTM-vsl		M25/CTM-basic	
$\boldsymbol{\varepsilon^c(\overline{\rho},\overline{u})}$	$X_{0.975}-E^a$	$X_{0.025}-E^a$	$X_{0.975}-E^a$	$X_{0.025}-E^a$	$X_{0.975}-E^a$	$X_{0.025}-E^a$	$X_{0.975}-E^a$	$X_{0.025}-E^a$
Min.	-5.0	-23.1	-10.7	-19.2	1.2	-7.4	1.4	-9.1
25th Q	-0.1	-11.9	1.8	-9.4	2.3	-4.7	3.8	-5.2
Mean	1.9	-8.8	3.5	-7.3	4.5	-3.8	5.0	-4.4
Median	1.1	-9.0	3.2	-6.9	4.9	-3.9	4.8	-4.2
75th Q	2.7	-5.6	5.0	-5.2	5.8	-3.1	6.4	-3.5
Max.	17.9	0.9	19.7	0.5	8.5	0.1	10.5	-0.7
$\boldsymbol{\varepsilon^v(\overline{\rho},\overline{u})}$	$X_{0.975}-E^a$	$X_{0.025}-E^a$	$X_{0.975}-E^a$	$X_{0.025}-E^a$	$X_{0.975}-E^a$	$X_{0.025}-E^a$	$X_{0.975}-E^a$	$X_{0.025}-E^a$
Min.	-6.2	-20.5	-16.5	-25.4	-0.6	-8.9	1.0	-10.6
25th Q	0.2	-12.4	2.1	-10.0	4.3	-4.0	4.7	-4.4
Mean	2.4	-9.7	4.5	-7.9	5.7	-2.6	5.9	-3.7
Median	2.4	-10.0	4.0	-7.2	5.7	-3.2	5.8	-3.7
75th Q	4.0	-7.1	6.4	-5.2	7.4	-1.7	7.0	-2.4
Max.	21.1	0.9	23.3	2.1	13.4	8.9	12.1	2.2

5. Conclusion

This paper has developed a data-driven five-phase methodological framework to study the propagation of uncertainties in a well-developed and commonly used discretised first-order macroscopic traffic flow model, the Cell Transmission Model (CTM), to uncertainties in average speed-based emission predictions. The developed methodology allows quantifying uncertainty in CTM model outputs using an ensemble-based optimisation approach. The quantification allows errors in both calibrated and validated CTM model outputs to be estimated and separately propagated to average speed-based emission predictions using a grid-based Monte Carlo sampling approach. The developed methodology enables the calculation of confidence intervals in emission predictions and their visualisation across the entire feasible region of CTM model outputs.

The operation of Variable Speed Limits (VSL) on road networks and the availability of VSL data have allowed examining both the basic CTM model formulation (CTM-basic) and the VSL-modified CTM model formulation (CTM-vsl). The ensemble-based optimisation of both CTM-vsl and CTM-basic on the same VSL-operated road network has shown that the CTM-vsl may not necessarily be appropriate to describe traffic behaviour for all time periods especially when VSL operation changes by time, loop detector, and by lane as it does for the selected road network. Nevertheless, the propagation of errors in the calibrated and validated CTM-vsl models to emission predictions are

similar to that of the CTM-basic models since the quantified uncertainties in both are similar for the same data set and road network.

The use of multiple data sets and different road networks have allowed to thoroughly test the proposed methodology and ensure transferability of findings. Across all road networks, highest variability has been observed for the supply parameters of CTM models in comparison to the demand parameters. Estimated errors in CTM model outputs have been observed to be road network specific and thus the final estimated confidence intervals in emission predictions depend on the road network. Estimated errors of traffic density and traffic speed, however, for any road network are unsurprisingly higher for validated CTM models in comparison to calibrated CTM model. Nevertheless, the propagation of the higher errors of validated CTM models to emission predictions does not necessarily give larger confidence intervals with the same magnitude of calibrated CTM models; a result of nonlinearity of the used emission model. While the mean additive upper bounds have been seen to be systematically higher (i.e. for all three road networks) based on estimated validation errors by a factor of 1.25 in comparison to those based on estimated calibration errors, additive lower bounds are not necessarily higher for all road networks.

This paper highlighted that the uncertainty captured in key components of CTM can be due to the lack of perfect representation of the CTM of the aggregate traffic behaviour such as the simplified fundamental diagram, steady-state speed-density relationship, and ignored influence of multiple vehicle classes, lane drops, and lane changing. However, captured uncertainty can also be due to uncertainties in input data and assumptions being made during the ensemble-based optimisation phase of the methodology. Particularly:

- The data transformation required for the input data such as the use of weighted average traffic speed based on the measured time-mean traffic speed rather than space-mean traffic speed which is considered a limitation of most of current traffic measurement networks installed on roadways. Another data transformation is the interpolation of 1-minute input data (typical resolution of traffic measurement systems) in order to match the resolution of the CTM model.

- The optimisation problem almost always relies on data which is of lower spatial and temporal resolution to that of the CTM model outputs. Incomplete spatiotemporal information provided to the optimisation algorithm can lead to uncertainties around the 'global' optimal solution for the problem if one exists.
- The significance level used for the statistical inference approach to selecting *top-solutions* has an influence on the captured variability in the parameter vector. While relaxing this assumption can reduce type-I error (rejecting a solution that should not be rejected) it can lead to increased type-II error (not rejecting a solution that should be rejected) and vice versa.

Despite the above, the developed methodology of uncertainty propagation from the CTM to average speed-based emission predictions can still be applied given any variation to the assumptions being made whether model structure assumptions (e.g. the use of multi-class CTM or higher order traffic flow models), input data assumptions (e.g. use of higher traffic measurement spatiotemporal resolution), and/or *top-solutions* criteria selection (e.g. increasing/decreasing the chosen significance level).

The lower resolution of measurements also implicates that error in the CTM-predicted traffic density and traffic speed is estimated based on spatiotemporal aggregate measurements rather than the resolution of the CTM-predictions themselves. While the captured error distributions can be either underestimated or overestimated, the developed methodology can still be applied with a higher spatiotemporal measurement resolution to improve upon the final confidence interval estimate of emission predictions.

In this paper, the developed methodology has focussed on propagating uncertainty in the outputs of a macroscopic traffic flow model to average speed-based emission predictions. This is considered the foundation for better understanding the complex and nonlinear four-step modelling chain (or five-step modelling chain if traffic assignment models are integrated with traffic flow models) which typically ends with modelling human exposure to traffic-related air pollutants. Uncertainties in average speed-based emission predictions, however, are not only dependent on

traffic data input (or traffic flow model outputs) but also on other inputs (mainly vehicle proportions) and on emission factor functions nested within the emission model structure itself which also need to be taken into consideration if this work is to be extended to the next modelling step of the chain. For instance, average speed-based emission models such as COPERT are nonlinear functions parameterised by vehicle class, fuel type, and standard-specific without any consideration of individual driving behaviour. It is also noteworthy that average speed-based emission models, such as COPERT, were originally developed as functions of trip-based average speed rather than link-based average speed which is how they are commonly implemented. Lastly, average speed-based emission models can be limited in terms of their applicability to very high resolution spatial and temporal traffic data which is the case for discretised macroscopic traffic flow models. This indicates the complexity of studying errors and uncertainties in such a complex modelling chain; starting from the first modelling step is key to better understand the final outputs of the modelling chain.

Acknowledgments

The authors would like to thank Highways England for providing access to the MIDAS traffic and Variable Speed Limit databases. The authors would also like to thank Dr Dong Ngoduy and the anonymous reviewers on their valuable input to this paper. Also, part of this work was undertaken on ARC2, part of the High Performance Computing (HPC) facilities at the University of Leeds, UK.

REFERENCES

Bai S, Chiu YCE, Niemeier DA (2007) A comparative analysis of using trip-based versus link-based traffic data for regional mobile source emissions estimation. *Atmospheric Environment*, *41*(35):7512-7523.

Bihorel S, Baudin M (2015) neldermead: R port of the Scilab neldermead module. R package version 1.0-10. http://CRAN.R-project.org/package=neldermead

Chiou YC, Huang YF, Lin PC (2012) Optimal variable speed-limit control under abnormal traffic conditions. *Journal of the Chinese Institute of Engineers*, *35*(3):299-308.

Cullen AC, Frey HC (1999) *Probabilistic techniques in exposure assessment: a handbook for dealing with variability and uncertainty in models and inputs*. Springer Science & Business Media.

Daganzo CF (1994) The cell transmission model: A dynamic representation of highway traffic consistent with the hydrodynamic theory. *Transportation Research Part B: Methodological*, 28(4):269-287.

Daganzo CF (1995) The cell transmission model, part II: network traffic. *Transportation Research Part B: Methodological*, 29(2):79-93.

DEFRA (2014) UK NAEI – National Atmospheric Emissions Inventory [online]. (Accessed 01.09.16.) Available from: http://naei.defra.gov.uk/

Department for Transport (2016) Traffic Counts – Transport Statistics [online]. (Accessed 01.09.16.) Available from: http://www.dft.gov.uk/traffic-counts/.

Dervisoglu G, Gomes G, Kwon J, Horowitz R, Varaiya P (2009) Automatic calibration of the fundamental diagram and empirical observations on capacity. In *Transportation Research Board 88th Annual Meeting (Vol. 15)*.

Eberhart RC, Kennedy J (1995) A new optimizer using particle swarm theory. In *Proceedings of the 6th International Symposium on Micro Machine and Human Science,* 1:39-43.

Feldman O, Maher M (2002) Optimisation of traffic signals using a cell transmission model. *In 34th Annual Universities' Transport Study Group Conference, Napier University, Edinburgh.*

Frey HC, Burmaster DE (1999) Methods for characterizing variability and uncertainty: comparison of bootstrap simulation and likelihood-based approaches. *Risk Analysis*, 19(1):109-130.

Gkiotsalitis K, Chow A (2014) Significance of fundamental diagrams to first-order macroscopic traffic modelling. *International Journal of Transportation*, 2(2):15-32.

Gomes G, Horowitz R, Kurzhanskiy AA, Varaiya P, Kwon J (2008) Behaviour of the cell transmission model and effectiveness of ramp metering. *Transportation Research Part C: Emerging Technologies, 16*(4):485-513.

Hadiuzzaman M, Qiu TZ (2013) Cell transmission model based variable speed limit control for freeways. *Canadian Journal of Civil Engineering*, 40(1):46-56.

Hegyi A, De Schutter B, Hellendoorn J (2005) Optimal coordination of variable speed limits to suppress shock waves. *IEEE Transactions on Intelligent Transportation Systems*, 6(1):102-112.

Helbing D (1996) Gas-kinetic derivation of Navier-Stokes-like traffic equations. *Physical Review E*, 53(3):2366.

Hoogendoorn SP, Bovy PH (2001) State-of-the-art of vehicular traffic flow modelling. *Proceedings of the Institution of Mechanical Engineers, Part I: Journal of Systems and Control Engineering*, 215(4):283-303.

Int Panis L, Broekx S, Liu R (2006) Modelling instantaneous traffic emission and the influence of traffic speed limits. *Science of the Total Environment*, 371(1):270-285.

Kimms A, Maassen KC (2011) Optimization and simulation of traffic flows in the case of evacuating urban areas. *OR spectrum*, *33*(3):571-593.

Kini MD, Frey HC (1997) *Probabilistic evaluation of mobile source air pollution: Volume 1, probabilistic modeling of exhaust emissions from light duty gasoline vehicles* (No. Final Report).

Kühlwein J, Friedrich R (2000) Uncertainties of modelling emissions from road transport. *Atmospheric Environment*, *34*(27):4603-4610.

Li J, Chen QY, Wang H, Ni D (2012) Analysis of LWR model with fundamental diagram subject to uncertainties. *Transportmetrica*, *8*(6):387-405.

Li Z, Liu P, Xu C, Wang W (2015) Optimal Mainline Variable Speed Limit Control to Improve Safety on Large-Scale Freeway Segments. *Computer-Aided Civil and Infrastructure Engineering*.

Lighthill MJ, Whitham GB (1955a) On kinematic waves I: Flood movement in long rivers. In *Proceedings of the Royal Society of London A: Mathematical, Physical and Engineering Sciences,* 229(1178):281-316.

Lighthill MJ, Whitham GB (1955b) On kinematic waves II: A theory of traffic flow on long crowded roads. In *Proceedings of the Royal Society of London A: Mathematical, Physical and Engineering Sciences,* 229(1178):317-345.

Lin J, Ge YE (2006) Impacts of traffic heterogeneity on roadside air pollution concentration. *Transportation Research Part D: Transport and Environment*, 11(2):166-170.

Liu S, De Schutter B, Hellendoorn H (2014) Integrated traffic flow and emission control based on FASTLANE and the multi-class VT-macro model. In *Proceedings of the European Control Conference (ECC)*, 2908-2913. *IEEE.*

Lo HK, Szeto WY (2002) A cell-based dynamic traffic assignment model: Formulation and properties. *Mathematical and Computer Modelling*, *35*(7):849-865.

Loecher M, Ropkins K (2015). RgoogleMaps and loa: Unleashing R Graphics Power on Map Tiles. *Journal of Statistical Software,* 63(4):1-18. URL http://www.jstatsoft.org/v63/i04/

Michalewicz Z (1994) GAs: What are they? In *Genetic algorithms + data structures = evolution programs*. Springer Berlin Heidelberg, 13-30.

MIDAS (2016) MIDAS Data – Mott MacDonald [online]. (Accessed 01.09.16.) Available from: https://www.midas-data.org.uk/.

Morgan MG, Henrion M, Small M (1992) *Uncertainty: a guide to dealing with uncertainty in quantitative risk and policy analysis*. Cambridge university press.

Muñoz L, Sun X, Sun D, Gomes G, Horowitz R (2004) Methodological calibration of the cell transmission model. In *Proceedings of the American Control Conference*, 1:798-803. IEEE.

Namdeo A, Mitchell G. Dixon R (2002) TEMMS: an integrated package for modelling and mapping urban traffic emissions and air quality. *Environmental Modelling & Software*, 17(2):177-188.

Nejadkoorki F, Nicholson K, Lake I. Davies T (2008) An approach for modelling CO_2 emissions from road traffic in urban areas. *Science of the Total Environment*, 406(1):269-278.

Nelder JA, Mead R (1965) A simplex method for function minimization. *The Computer Journal*, 7(4):308-313.

Newell GF (1993) A simplified theory of kinematic waves in highway traffic, part I: General theory. *Transportation Research Part B: Methodological*, 27(4):281-287.

Newell GF (2002) A simplified car-following theory: a lower order model. *Transportation Research Part B: Methodological*, 36(3):195-205.

Ngoduy D (2011) Multiclass first-order traffic model using stochastic fundamental diagrams. *Transportmetrica*, 7(2):111-125.

Ngoduy D, Maher MJ (2012) Calibration of second order traffic models using continuous cross entropy method. *Transportation Research Part C: Emerging Technologies*, 24:102-121.

Ni D, Leonard J, Guin A, Williams B (2004) Systematic approach for validating traffic simulation models. *Transportation Research Record: Journal of the Transportation Research Board*, 1876:20-31.

Ntziachristos L, Samaras Z, Eggleston S, Gorissen N, Hassel D, Hickman AJ, Joumard R, Rijkeboer R, White L, Zierock L (2000) *Validation of road vehicle and traffic emission models, a review and meta-analysis: COPERT IV Computer Programme to Calculate Emissions From Road Transport, Methodology and Emissions Factors (Version 2.1)*. Technical Report No. 49. European Environment Agency.

Papageorgiou M, Kosmatopoulos E, Papamichail I (2008) Effects of variable speed limits on motorway traffic flow. *Transportation Research Record: Journal of the Transportation Research Board*, 2047:37-48.

Payne HJ (1971) Models of freeway traffic and control. *Mathematical models of public systems*.

Poole AJ, Kotsialos A (2012) METANET model validation using a genetic algorithm. *IFAC Proceedings Volumes*, 45(24):7-12.

Poole A, Kotsialos A (2016) Swarm intelligence algorithms for macroscopic traffic flow model validation with automatic assignment of fundamental diagrams. *Applied Soft Computing*, 38:134-150.

R Core Team (2015) R: A language and environment for statistical computing. R Foundation for Statistical Computing, Vienna, Austria. URL http://www.R-project.org/

Rakha H, Ahn K (2004) Integration modelling framework for estimating mobile source emissions. *Journal of transportation engineering*, 130(2):183-193.

Richards PI (1956) Shock waves on the highway. *Operations research*, 4(1):42-51.

Samaranayake S, Glaser S, Holstius D, Monteil J, Tracton K, Seto E, Bayen A (2014) Real-Time Estimation of Pollution Emissions and Dispersion from Highway Traffic. *Computer-Aided Civil and Infrastructure Engineering*, 29(7):546-558.

Samaras C, Tsokolis D, Toffolo S, Garcia-Castro A, Vock C, Ntziachristos L, Samaras Z (2014) Limits of applicability of COPERT model to short links and congested conditions. In *Proceedings of the 20th International Transport and Air Pollution Conference.*

Sarkar D (2008) Lattice: Multivariate Data Visualization with R. Springer, New York. ISBN 978-0-387-75968-5.

Shorshani MF, André M, Bonhomme C, Seigneur C (2015) Modelling chain for the effect of road traffic on air and water quality: techniques, current status and future prospects. *Environmental Modelling & Software*, 64:102-123.

Spiliopoulou A, Kontorinaki M, Papageorgiou M, Kopelias P (2014) Macroscopic traffic flow model validation at congested freeway off-ramp areas. *Transportation Research Part C: Emerging Technologies*, 41:18-29.

Spiliopoulou A, Papamichail I, Papageorgiou M, Tyrinopoulos I, Chrysoulakis J (2015) Macroscopic traffic flow model calibration using different optimization algorithms. *Transportation Research Procedia*, 6:144-157.

Sumalee A, Zhong RX, Pan TL, Szeto WY (2011) Stochastic cell transmission model (SCTM): a stochastic dynamic traffic model for traffic state surveillance and assignment. *Transportation Research Part B: Methodological*, 45(3):507-533.

Treiber M, Kesting A (2012) Validation of traffic flow models with respect to the spatiotemporal evolution of congested traffic patterns. *Transportation Research Part C: Emerging Technologies*, 21(1):31-41.

Wismans L, Van Berkum E, Bliemer M (2011) Modelling externalities using dynamic traffic assignment models: A review. *Transport Reviews*, 31*(*4):521-545.

Zhang, L, Yin Y, Chen S (2013) Robust signal timing optimization with environmental concerns. *Transportation Research Part C: Emerging Technologies*, 29:55-71.

Zhong R, Chen C, Chow AH, Pan T, Yuan F, He Z (2015) Automatic calibration of fundamental diagram for first-order macroscopic freeway traffic models. *Journal of Advanced Transportation*, 50(3):363-385.

Zhou X, Tanvir S, Lei H, Taylor J, Liu B, Rouphail NM, Frey HC (2015) Integrating a simplified emission estimation model and mesoscopic dynamic traffic simulator to efficiently evaluate emission impacts of traffic management strategies. *Transportation Research Part D: Transport and Environment*, 37:123-136.

Zhu F, Lo HK, Lin HZ (2013) Delay and emissions modelling for signalised intersections. *Transportmetrica B: Transport Dynamics*, 1(2):111-135.